



Published in final edited form as:

Graefes Arch Clin Exp Ophthalmol. 2013 October ; 251(10): 2299–2309. doi:10.1007/s00417-013-2296-5.

Disruption of the human cone photoreceptor mosaic from a defect in NR2E3 transcription factor function in young adults

Sung Pyo Park,

Department of Ophthalmology, Columbia University, New York, NY, USA

Department of Ophthalmology, Kangdong Sacred Heart Hospital, Hallym University Medical Center, Seoul, South Korea

In Hwan Hong,

Department of Ophthalmology, Kangdong Sacred Heart Hospital, Hallym University Medical Center, Seoul, South Korea

Stephen H. Tsang,

Department of Ophthalmology, Columbia University, New York, NY, USA

Department of Pathology & Cell Biology, Columbia University, New York, NY, USA

Departments of Ophthalmology, Pathology and Cell Biology, Edward S. Harkness Eye Institute, Columbia University, 635 west 165th street, New York, NY 10032, USA

Winston Lee,

Department of Ophthalmology, Columbia University, New York, NY, USA

Jason Horowitz,

Department of Ophthalmology, Columbia University, New York, NY, USA

Suzanne Yzer,

Rotterdam Eye Hospital, Rotterdam, Netherlands

Rando Allikmets, and

Department of Ophthalmology, Columbia University, New York, NY, USA

Department of Pathology & Cell Biology, Columbia University, New York, NY, USA

Stanley Chang

Department of Ophthalmology, Columbia University, New York, NY, USA

Sung Pyo Park: sungpyo@hallym.or.kr; In Hwan Hong: loperter@hanmail.net; Stephen H. Tsang: sht2@columbia.edu; Winston Lee: winstonlee219@gmail.com; Jason Horowitz: jh3177@columbia.edu; Suzanne Yzer: S.Yzer@oogziekenhuis.nl; Rando Allikmets: rla22@columbia.edu; Stanley Chang: sc434@mail.cumc.columbia.edu

Abstract

Background—Enhanced S-cone syndrome is an orphan disease caused by mutations in the *NR2E3* gene which result in an increased number of S-cones overpopulating the retina. Although

the characteristic onset of enhanced S-cone syndrome can be well-documented by current ophthalmic imaging modalities, techniques such as spectral-domain optical coherence tomography (SD-OCT) and scanning laser ophthalmoscopy (SLO) fail to provide sufficient details regarding the microstructure of photoreceptors in retinal diseases. Adaptive optics (AO) provides a unique opportunity to analyze the effects of genetic mutations on photoreceptors by compensating aberrations of human eyes.

Methods—Three eyes of three young adults with enhanced S-cone syndrome were studied by clinical examination, genetic screening, fundus autofluorescence (FAF) imaging, SD-OCT, and electroretinography (ERG). Cone mosaic imaging was accomplished by an AO-SLO equipped with a dual crystal on silicon spatial light modulator. Qualitative image analyses and genetic findings were investigated in each patient.

Results—The diagnosis of patients was confirmed by ERG finding. Genetic screening confirmed the presence of two disease-causing mutations in the *NR2E3* gene in each study patient, as well as identified a novel mutation (202 A > G, S68G). Fundus photograph, FAF, and SD-OCT found rosette-like lesion within the mid-periphery along the vascular arcades of the retina. In all AO-SLO images of patients, sparse distribution and asymmetric size of cone mosaic pattern were found within central retina. There were regions of dark space between groups of photoreceptors, distinguishable from shadowing and artifacts.

Conclusions—AO-SLO provided an in-depth window into the retina of live enhanced S-cone syndrome patients beyond the ability of other current imaging modalities. Dark lesions within the central retina in each patient contain structurally dysfunctional cones which account for retinal mosaic disorganization, and may predispose affected areas to other abnormalities such as rosette lesions. AO-SLO can be an efficient diagnostic tool in clinics for examining cellular-level pathologies in various retinal dystrophies.

Keywords

Adaptive optics scanning laser ophthalmoscopy (AO-SLO); Enhanced S-cone syndrome (ESCS); Photoreceptor layer

Introduction

Enhanced S-cone syndrome (ESCS) is a rare slowly progressive, autosomal recessive disorder caused by *NR2E3* gene mutations. These genetic alterations result in an increased number of S-cones, which overpopulate the retina at the expense of other photoreceptor types (L- and M-cones, rod cells) [1–5]. Patients with ESCS show night blindness, variable visual acuity loss, and visual field defects. The ESCS fundus is characterized by pigmented deposits, primarily along vascular arcades, and intraretinal cystoid lesions that often involve the macula. Milam et al. examined a postmortem retina from a patient with ESCS caused by a homozygous mutation (R311Q) in *NR2E3*. They observed a dramatic increase in the S-cone population and a 2-fold increase in the overall number of cones [6]. Additionally, they were unable to identify any rods [6]. Even though the morphology of ESCS has been well-studied, disease pathogenic mechanisms remain largely unknown. Retinal functionality is consistent with morphological findings. In full-field electroretinography (ERG) findings, L- and M-cone signals were severely reduced and S-cone signals were hypersensitive [7, 8].

Furthermore, rod responses were undetectable and the maximal dark-adapted response closely mimicked single-cone responses. Both dark- and light-adapted ERG waveforms are consistent with those of a retina that is dominated by S-cones [9]. However, ESCS diagnoses can be established without specific short-wavelength stimulation and S-cone-specific ERG is not commonly performed.

Although the onset of ESCS can be well-documented by current ophthalmic imaging modalities, techniques such as spectral-domain optical coherence tomography (SD-OCT) and scanning laser ophthalmoscopy (SLO) fail to provide sufficient imaging detail. Because of optical aberrations of the human eye, the microstructure of photoreceptors cannot be viewed with these techniques. Adaptive optics (AO) can be combined with SLO to compensate for these aberrations, utilizing wavefront sensors to measure ocular aberrations and a deformable mirror or spatial light modulator to correct for them [10–14]. These corrections allow individual cones to be imaged [15, 16]. Integrated AO and SLO (AO-SLO) yields retinal images with high resolution and contrast [11, 17], providing a unique opportunity to study the effects of genetic mutations on individual photoreceptors in vivo [17–21].

In the present study, we identified *NR2E3* mutations in three live young adult patients; one of the mutations is novel and unpublished. All three patients were diagnosed with ESCS using standard ERG results. Patients underwent examination with various retinal imaging techniques, including fundus photography, fundus autofluorescence (FAF), OCT, and compact AO-SLO (dual liquid-crystal phase modulator) [22]. Non-invasive SLO-AO can image individual photoreceptor structural abnormalities in patients with *NR2E3* mutation retinal degenerations.

Materials and methods

Participants

The institutional review board of Columbia University reviewed and approved this prospective study (approvals AAII480, AAAB6560). All research procedures adhered to the tenets of the Declaration of Helsinki, and informed consent was obtained from each subject before any research procedures were performed. Compliance with the Health Insurance Portability and Accountability Act was maintained.

Twelve genetically confirmed cases of ESCS underwent regular follow-up examinations at the university clinic. Complete ophthalmic evaluations were performed on each subject, which included measurements of best-corrected visual acuity (BCVA), intraocular pressure, axial length, and subjective refraction. Further examinations included indirect ophthalmoscopy, slit-lamp examination with a contact lens, color fundus photography, infrared (IR) and fundus autofluorescence (FAF) imaging. The Spectralis HRA + OCT (Heidelberg Engineering, Heidelberg, Germany) allowed for simultaneous acquisition of *en face* infrared (IR), FAF, and high-resolution SD-OCT images, providing point-to-point correlations between the various types of retinal images. Inclusion criteria for the study cohort included stable fixation, the absence of macular cystic degeneration and posterior subcapsular cataracts, the absence of astigmatism (greater than 2.5 D) and 20/60 or better

BCVA in the study eye. Patients who had difficulty complying with the AO-SLO imaging protocol were also excluded. Of the twelve patients referred, nine were excluded leaving, three for this study.

After pupil dilation (topical 1 % tropicamide), retinal function was assessed using full-field scotopic and photopic ERG recordings. Both scotopic and photopic ERGs were obtained from both eyes with silver-impregnated fiber electrodes (DTL, Diagnosys LLC, Littleton, MA, USA), according to the International Society for Clinical Electrophysiology of Vision (ISCEV) standards [23]. The recording protocol incorporated rod-specific and standard bright-flash ERGs, both of which were recorded after a minimum dark adaptation time of 20 min. Photopic 30-Hz flicker stimulus and transient photopic cone ERGs were recorded after 10 min of light adaptation [24].

Genetic analysis

Blood samples were genetically screened for *NR2E3* coding region mutations that cause disease (PreventionGenetics, Marshfield, WI, USA). The total genomic DNA was extracted from peripheral blood samples with the QIAamp DNA Mini Kit (Qiagen Inc., Valencia, CA, USA). All eight exons and flanking intronic regions of the *NR2E3* gene were directly sequenced on the ABI 3100XL DNA sequencer (Applied Biosystems, Inc. [ABI], Foster City, CA, USA) using a Big Dye Terminator Labeling Kit (ABI), as previously described [25]. Detected variants were compared to the *NR2E3* mutation database (Human Gene Mutation Database, <http://www.hgmd.cf.ac.uk/ac/gene.php?gene=NR2E3>), and analyzed for evolutionary conservation by the prediction programs, PolyPhen2 and SIFT.

Adaptive optics scanning laser ophthalmoscopy

As previously described by Hirose et al., the AO-SLO system is composed of the following components: (1) light sources for imaging and aberration measurement, (2) an optical system, (3) the AO system, (4) a scanner, and (5) the data acquisition and image composition system [22]. The two light sources used in this system were a superluminescent diode (wavelength: 840 ± 25 nm, S840-B-I-20; Superlum, Ireland) used for imaging and the beacon light, another superluminescent diode (wavelength: 760 ± 5 nm, QSDM-760-2, QPhotonics, USA) used for measuring aberrations. Consistent with the American National Standards Institute (ANSI) safety limits, the imaging and beacon light power levels were set to 450 and 40 μ W respectively. The imaging light was collimated through a fiber coupler and a single-mode fiber. It propagated along telescope optics via axially symmetric aspherical mirrors, arranged off-axis, to the dual liquid crystal on the silicon spatial light modulators (LCOS-SLMs, X10468-02; Hamamatsu Photonics, Japan). The LCOS-SLMs had an active area of 16×12 mm and 792×600 pixels, with a maximum stroke of 1λ (840 nm).

Two LCOS-SLMs modulated the polarized imaging light components to compensate for ocular wavefront aberrations. The aberrations were measured using the beacon light and a Hartmann–Shack wavefront sensor (HASO32-eye, Imagine Eyes, France). An 8-kHz resonant scanner (CRS 8 kHz; GSI Group, USA) created horizontal raster scans, while a Galvano scanner (VM500+; GSI Group, USA) scanned the imaging beam in the horizontal

direction. Data acquisition of the reflected light system was initiated when the imaging light was scanned. Light reflected from the retina was detected by an avalanche photodiode, and converted to an electrical signal, which was then amplified 10-fold by a commercial amplifier (SR560; Stanford Research Systems, USA). The Analog/Digital (AD) converter board simultaneously digitized the amplifier signals and the synchronized scanner signals at a rate of 15 MHz and 12 bits respectively. The digitized data were then recorded onto the hard disk of a personal computer over a period of approximately 2 s. The final SLO output image size was 400×400 pixels (32 frames per second). Images were obtained at multiple locations within 1.5 mm from the center of the fovea, with cone cells appearing as bright spots, 2–5 μm or above in diameter. A montage of AO-SLO images was created by selecting the area of interest and creating an image overlay. Each montage was then verified by visual examination, and cross-comparison to pre-collected wide-field images was performed.

Results

The demographic characteristics of each study subject and examined eye are summarized in Table 1. None of the three patients examined exhibited any underlying systemic disease, lens opacity, or inflammatory sign. A dilated fundus examination in patient 1 revealed extensive subretinal nummular pigmentation, largely located in the mid-periphery along the vascular arcades (Fig. 1). This characteristic pigment clumping was also noted in all other ESCS patients. There was no evidence of peripheral or central retinoschisis or maculopathy, and no additional abnormal findings were found within the vascular arcades. The FAF images showed hypo-autofluorescent areas coinciding with dark pigment clumping along the vascular arcade (Fig. 2a, b). Nummular pigmentation along the vascular arcades was also observed on an IR image from patient 3 (Fig. 2c). Posterior pole autofluorescence was unremarkable for all patients, except patient 2, who had some hyper-autofluorescent areas within the parafovea. These were most prominent just nasal to the macula.

None of the patients had SD-OCT findings of cystoid macular edema or foveal schisis (Fig. 2), although the overall thickness of the retina was decreased. These SD-OCT images also showed an intact inner ellipsoid band, indicating the presence of photoreceptor inner/outer segment junctions (IS/OS junctions). Photoreceptor outer segments, retinal pigment epithelium (RPE), and Bruch's membrane were also intact in all patients. In patient 2, SD-OCT images did not show any anatomic abnormalities that corresponded to the hyper-autofluorescent lesion seen on IR images (Fig. 2b). Patient 3 did have a slightly disrupted IS/OS line in the parafoveal area, along with distinct white spots, subretinal fibrosis, and perimacular atrophy within the pigmented area (Fig. 2c). An area of nummular pigmentation was selectively cross-sectioned and examined for anatomic abnormalities, consistent with those seen in patient 2 (Fig. 3a). Differing from pigmented lesions, which have a dark color and are round in shape, SD-OCT showed a lesion with an outer retinal tubulation and a rosette-like shape (Fig. 3b).

All of the patients exhibited the characteristic ISCEV-standardized ERG waveforms associated with ESCS (Fig. 4). Rod-specific ERGs were not detectable, and the maximal dark-adapted rod-cone response waveforms were identical to single flash cone response waveforms in shape, but the magnitude differed. Additionally, single-cone responses

exhibited an implicit delay. The 30-Hz flicker stimulus ERG was also delayed and its b-wave had a lower amplitude than the a-wave of single flash cone responses.

Each patient was screened for mutations in the *NR2E3* gene by direct sequencing of all eight exons. Two compound heterozygous and homozygous mutations were found in each patient, including two disease-associated mutations in two patients. These were missense variant 202 A > G (S68G) and nonsense variant 363 C > T (R125X, Table 1), both of which occurred in conserved gene sequences. In addition, the S68G variant was predicted to be damaging by the PolyPhen (score 0.98) and SIFT programs. The other mutations found (Table 1) are disease-associated variants and included the splicing variant IVS1–2A > C and the R311Q mutation.

Cones from a normal retina on AO-SLO images resemble bright, oval-shaped dots packed in a uniform arrangement (Figs. 5c and 6a). Although the cone packing arrangement in ESCS patients was less discernible, the physical arrangement of cones was disrupted (Figs. 5b and 6). There also appeared to be a large variation in signal intensity from each identifiable cone, compared to the more homogenous mosaic of the normal retina. Interestingly, the cones in ESCS patients appeared larger than cones imaged from normal subjects. Additionally, compared to normal eyes, cone cells were distributed more sparsely in ESCS eyes, and dark patchy-like lesions in the macula seemed to further interfere with the cone mosaic. These dark areas were more apparent in color-inverted images, and in images where individual cones were automatically labeled with the software analysis program (Fig. 6). A similar labeled image from a normal patient showed no dark lesions or patches. Hypo-reflective patches were distinguishable from blood vessel shadowing and retinal folds (as observed in color fundus photographs or SD-OCT images) by their size, shape, and tendency to appear in clusters. These patch lesions were not observed to be present in the normal foveal avascular zone where blood vessel shadowing is typically absent. The ellipsoid inner segment band on SD-OCT images, which represents the photoreceptor IS/OS junction, was intact in eyes that had multiple dark central retinal lesions on AO-SLO images (Fig. 7).

Discussion

Nummular pigmented clumping along the vascular arcades, along with the classic retinal phenotype of adult ESCS patients, was observed in each of our three patients. Foveal cystic degeneration, which can be present in young ESCS patients [26, 27], was not observed. Even though nummular pigmentary retinopathy is largely consistent with ESCS, ISCEV-standardized ERG results and genetic screening were the main diagnostic determinants in each study patient. Scone-specific ERGs were not necessary for diagnosis in our study patients because ISCEV full-field ERG findings were sufficient to document the diagnosis of ESCS. Although patient 1 exhibited the least remarkable findings in FAF and OCT, her ERG responses were immeasurably extinguished. This severe attenuation of electrophysiological function is probably attributable to the severe pigmented degeneration in the peripheral retina, as in Fig. 1, an area that not accessed by FAF and OCT measurements which are limited posterior pole of the retina.

Patient 3 showed R311Q homozygosity, which is a common cause of ESCS [28]. A prospective study by Pachydaki et al. documented phenotypic characteristics of several R311Q cases, including round, pigmented clumping along the retinal mid-periphery, which is consistent with our findings [28]. The fundus of patient 3 was extensively scarred and marked with white spots, as seen in the IR and SD-OCT images. Through the multimodal imaging assessment of patient 3, we realized that these white spots were different from pigmented lesion, subretinal scarring, and atrophy. Our clinical findings are in agreement with those of a mouse model (*NR2E3^{rd7}*), which harbors a deletion in *NR2E3* [9, 29]. The white spots, observed on the color fundus photos in both the *NR2E3^{rd7}* and patient 3, can be associated with the hyper-autofluorescent spots seen in FAF macular imaging. A recent study conducted by Wang et al. showed that these hyper-autofluorescent spots, defined as rosettelike lesions, reflect the disruption of the photoreceptor layer, and correspond to the emergence of macrophages [26]. From the literature and our study results, we confirm that the white spot is a rosette-like lesion, and we assume that these lesions are a finding specific to ESCS.

Sequencing the specific *NR2E3* coding region allowed identification of the Ser68Gly (S68G) substitution (202A>G) in patient 2. This missense mutation has not been reported in previous studies [1, 2, 5, 6, 24, 26]. Typical numerous subretinal pigmented lesions were seen in this patient, but there were no abnormal appearances in the macular area. Although FAF did show some hyper-autofluorescence within the parafoveal area, the overall retinal structure and thickness were normal, as viewed and measured on SD-OCT images. Due to patient 2's young age and disease stage, further multimodal assessments overtime, which should include SD-OCT and AO-SLO, would be needed to reveal the phenotypic characteristics and disease progression of this novel *NR2E3* mutation.

Instead of using a deformable mirror to correct for wavefront aberrations, the AO system used in this study was equipped with a dual LCOS-SLM that served as a wavefront corrector. This AO-SLO system sufficiently compensated for aberrations and improved SLO image contrast, while still performing high-speed imaging [21]. These advantages have led us to believe that AO-SLO may some day become practical for clinical use. With this dual AO system, we observed sparse distribution and multiple abnormal clusters within the cone mosaic in ESCS patients, which were not observed in normal eyes. Previous studies with AO systems have also reported abnormal cone mosaic patterns that were characterized by cone loss and pattern disruption with abnormal OCT results [9, 17, 30, 31]. However, the multiple dark lesions with disrupted cone mosaic patterns in our patients were accompanied by a relatively intact inner ellipsoid band on SD-OCT scans. Patient 3 had AO-SLO images that had a larger dark patchy lesion, compared to the other patients, and this may be correlated with the slight IS/OS junction disruption seen on SD-OCT images. To the best of our knowledge, this is the first in-vivo study of cone structure in living, young ESCS patients. These findings demonstrate the utility of AO-SLO analysis as a sensitive method for detecting disruptive effects in the cone mosaic of ESCS patients in the early stages of the disease. Furthermore, future studies utilizing this method may provide valuable in-vivo genotype–phenotype correlations in patients with known genetic mutations.

Mustafi et al. [32] demonstrated that the neural retina leucine zipper transcription factor-knockout (*Nrl*^{-/-}) mouse model exhibits many phenotypic features consistent with human ESCS. The retina of this experimental mouse also exhibits aberrant clustering of photoreceptors, with empty patches where nuclear rosettes had formed. Scanning electron microscopy revealed that cone-like photoreceptor packing in these *Nrl*^{-/-} mice was greatly reduced, compared to that of the wild-type (wt) mouse. Wang et al. [26] reported that rosettelike lesions in ESCS patients are associated with increased autofluorescence on FAF imaging, and are correlated with abnormal SD-OCT findings. These clinical findings have inspired the use of AO-SLO to further understand the cellular structure and organization of the ESCS mosaic. It is important to note that a limitation of the instrument used in this study was its inability to acquire live images of the peripheral retina—limiting our ability to assess the topological manifestation of resette-like lesions typically observed in SD-OCT scans. Histopathological and other imaging studies have suggested that increased central retinal photoreceptor outer nuclear layer (ONL) thickness, along with the presence of a macular hyper-autofluorescent ring, may be associated with retinal rosettes [24]. Overcoming the field of view limitation in our instrument may allow for the early detection of rosette-like lesion development in our patients, before these lesions appear on FAF or SD-OCT images.

A previous histological study of a 77-year-old patient with an *NR2E3* mutation showed a dramatic increase in the S-cone population and a 2-fold increase in the total number of cones [6]. Compared with mid and far peripheral retina, the central part of the macula did not contain a recognizable fovea, and the inner plexiform layer was interrupted by clusters of cells and radial fibers in this patient. Our study showed that dark patchy lesions prominently existed in the central area of retina as well. Based on these facts, we postulate that proliferation of S-cone cells occurs over the entire retina, and is followed by disruption of the normal photoreceptor mosaic, beginning in the central area. Alternatively, we suggest that there may only be a mosaic disruption, and that S-cone proliferation does not occur in the central area. Due to the limited understanding of *NR2E3* mutations and the lack of histopathological studies of ESCS patients, we can only postulate the pathogenesis of *NR2E3* mutations. Our study therefore suggests that fully understanding how these patch lesions appear in SD-OCT may require accompanying histopathological studies in patients with the *NR2E3* mutations, and continuous correlations between AO-SLO and SD-OCT images. Undertaking such studies in younger patients can yield greater understanding of the pathogenesis of ESCS, especially with respects to changes in cone cell proliferation and disruption over time.

Several limitations of our study should be mentioned. A previous histological study found that the total number of cones was increased in the *NR2E3* mutant retina compared with the normal retina [6]. Additionally, many previous AO studies have performed quantitative analysis on cone cell density and cone optical properties [16–21, 30, 31]. Unfortunately, neither manual nor automatic calculation methods for cone density have been developed for our AO-SLO system and we were not able to quantitatively evaluate the disrupted cone cells. Unlike the histological results obtained by Milam et al. [6], we expected a smaller cone density measurement from quantitative analyses because of the sparse distribution and multiple dark lesions. However, precise methods for determining cone density should be

involved in study analyses. Previous studies utilizing AO to investigate S-cone dystrophy have shown the absence of S-cones also coincides with disruptions in cone mosaic regularity [33]. Unfortunately, we were not able to classify individual cone types by comparing images taken of bleached photopigment, fully regenerated photopigment, and selective bleached photopigment by a 470 or 650 nm light. Another limitation of our study was a lack of functional assessments (e.g., full-field ERG, multifocal ERG) to reveal S-, L-, and M-cone distributions [34]. These limitations made it impossible for us to demonstrate the preservation or lack of L- and M-cones. We also could not distinguish them by size in AO-SLO images. However, we can postulate that trichromatic cone function and circuitry is unaffected in the central macula, because visual acuity was normal in all patients studied. Nonetheless, the ability to qualitatively monitor and observe changes in the living human retinal mosaic makes monitoring disease progression and investigating early disease mechanisms feasible. It also may validate the efficacy of novel interventions, such as gene replacement therapy, in earlier disease stages. In light of this expectation, current AO-SLO systems must be combined with not only quantitative data analysis methods for structural assessments, but also various kinds of ERG-collection strategies for functional assessments. Achieving this with our AO-SLO system may prove valuable in determining treatment efficacy of novel therapeutics by examining the cone survival rates in ESCS patients and in animal models of retinal disease.

In summary, through a multi-modular approach, which included gross (fundus photography, FAF) and microscopic (SD-OCT, AO-SLO) imaging, along with full-field ERG testing and genetic screening, we were able to provide a complete assessment of the clinical and genetic attributes of ESCS in young adult patients. While there have been many studies examining ESCS pathogenesis, less is understood about the patterning of cone differentiation and proliferation associated with the *NR2E3* mutation. In addition to identifying mutations associated with ESCS, we also observed dark patchy lesions in the parafoveal areas that were detected by our AO-SLO system. This feature of the disease has not been identified previously by other standard diagnostic imaging modalities, and not been associated with poor visual acuity. Our study has provided insight into the pathological consequences of ESCS on the organization of the cone mosaic. Since individual neurons, including the photoreceptors, are not suitable for biopsy, in-vivo single-cell imaging provides a unique opportunity to evaluate the effects of *NR2E3* mutations on ESCS patients. However, determining how these regions of patchy lesions and disrupted cones appear in SD-OCT will require histopathological studies of S-cone cells in patients with the *NR2E3* mutation. Additionally, as we conducted the study with younger patients, further, continuous correlations between AO-SLO and SD-OCT images will be needed to make a comprehensive functional and quantitative assessment of macular cone and rod distributions, which will be helpful in better understanding the pathogenic progression of *NR2E3* mutations.

Acknowledgement

Publication of this article was supported by multiple grants. These included the following: a Core Support for Vision Research grant (P30EY019007: SHT, RA) and National Eye Institute of The National Institutes of Health (Bethesda, MD, USA) grants (EY018213:SHT, EY019861: RA, SHT). Funds were also received from the Foundation Fighting Blindness (Owings Mills, MD, USA), as were unrestricted funds from Research to Prevent

Blindness Inc, (New York, NY, USA). Dr. Tsang is a fellow of the Burroughs– Wellcome Program in Biomedical Sciences, and has been supported by the following grants: the Bernard Becker Association of University Professors in Ophthalmology Research to Prevent Blindness Award, the Foundation Fighting Blindness, Dennis W. Jahnigen Award of the American Geriatrics Society, Joel Hoffman Scholarship, and the Crowley Family Fund and Barbara & Donald Jonas Family Funds. The authors have no financial support or conflicts of interest from the materials or methods used in this investigation. Individual author contributions: Design and conduct of study (SPP, IHH, SHT); management, analysis, and interpretation of data (SPP, IHH, WL, SY, SHT); and preparation, review and/or approval of manuscript (SPP, WL, SC, RA, JH, SHT). The authors thank Canon Inc. (Tokyo, Japan) for their technical support with the AO-SLO system, and Elena N. Bukanova for technical support and contributions with genetic analyses. Further gratitude is extended to Drs. Lawrence Yannuzzi and Irene Barbazetto for patient referral.

References

- Haider NB, Jacobson SG, Cideciyan AV, Swiderski R, Streb LM, Searby C, Beck G, Hockey R, Hanna DB, Gorman S, Duhl D, Carmi R, Bennett J, Weleber RG, Fishman GA, Wright AF, Stone EM, Sheffield VC. Mutation of a nuclear receptor gene, NR2E3, causes enhanced S-cone syndrome, a disorder of retinal cell fate. *Nat Genet.* 2000; 24:127–131. [PubMed: 10655056]
- Michaelides, M.; Holder, G.; Moore, AT. Inherited retinal dystrophies. In: Taylor, D.; Hoyt, GS., editors. *Pediatric ophthalmology and strabismus.* 2nd edn.. Elsevier Saunders; New York: 2005. p. 531-557.
- Fishman, GA. The enhanced S-cone syndrome. In: Fishman, GA.; Birch, DG.; Holder, GE.; Brigell, MG., editors. *Ophthalmology Monograph 2—Electrophysiologic Testing in Disorders of the Retina, Optic Nerve, and Visual Pathway.* 2nd edition.. Singapore: American Academy of Ophthalmology; 2001. p. 120
- Sharon D, Sandberg MA, Caruso RC, Berson EL, Dryja TP. Shared mutations in NR2E3 in enhanced S-cone syndrome, Goldmann–Favre syndrome, and many cases of clumped pigmentary retinal degeneration. *Arch Ophthalmol.* 2003; 121:1316–1323. [PubMed: 12963616]
- Hayashi T, Gekka T, Goto-Omoto S, Takeuchi T, Kubo A, Kitahara K. Novel NR2E3 mutations (R104Q, R334G) associated with a mild form of enhanced S-cone syndrome demonstrate compound heterozygosity. *Ophthalmology.* 2005; 112:2115. [PubMed: 16225923]
- Milam AH, Rose L, Cideciyan AV, Barakat MR, Tang WX, Gupta N, Aleman TS, Wright AF, Stone EM, Sheffield VC, Jacobson SG. The nuclear receptor NR2E3 plays a role in human retinal photoreceptor differentiation and degeneration. *Proc Natl Acad Sci USA.* 2002; 99:473–478. [PubMed: 11773633]
- Fishman GA, Peachey NS. Rod-cone dystrophy associated with a rod system electroretinogram obtained under photopic conditions. *Ophthalmology.* 1989; 96:913–918. [PubMed: 2787013]
- Kinori M, Pras E, Kolker A, Ferman-Attar G, Moroz I, Moisseiev J, Bandah-Rozenfeld D, Mizrahi-Meissonnier L, Sharon D, Rotenstreich Y. Enhanced S-cone function with preserved rod function: a new clinical phenotype. *Mol Vis.* 2011; 17:2241–2247. [PubMed: 21897746]
- Yoon MK, Roorda A, Zhang Y, Nakanishi C, Wong LJ, Zhang Q, Gillum L, Green A, Duncan JL. Adaptive optics scanning laser ophthalmoscopy images in a family with the mitochondrial DNA T8993C mutation. *Invest Ophthalmol Vis Sci.* 2009; 50:1838–1847. [PubMed: 18997096]
- Liang J, Williams DR, Miller DT. Supernormal vision and high-resolution retinal imaging through adaptive optics. *J Opt Soc Am A Opt Image Sci Vis.* 1997; 14:2884–2892. [PubMed: 9379246]
- Roorda A, Romero-Borja F, Donnelly Iii W, Queener H, Hebert T, Campbell M. Adaptive optics scanning laser ophthalmoscopy. *Opt Express.* 2002; 10:405–412. [PubMed: 19436374]
- Roorda A, Williams DR. The arrangement of the three cone classes in the living human eye. *Nature.* 1999; 397:520–522. [PubMed: 10028967]
- Roorda A, Williams DR. Optical fiber properties of individual human cones. *J Vis.* 2002; 2:404–412. [PubMed: 12678654]
- Pallikaris A, Williams DR, Hofer H. The reflectance of single cones in the living human eye. *Invest Ophthalmol Vis Sci.* 2003; 44:4580–4592. [PubMed: 14507907]
- Zhang Y, Poonja S, Roorda A. MEMS-based adaptive optics scanning laser ophthalmoscopy. *Opt Lett.* 2006; 31:1268–1270. [PubMed: 16642081]
- Zhang Y, Roorda A. Evaluating the lateral resolution of the adaptive optics scanning laser ophthalmoscope. *J Biomed Opt.* 2006; 11:014002. [PubMed: 16526879]

17. Merino D, Duncan JL, Tiruveedhula P, Roorda A. Observation of cone and rod photoreceptors in normal subjects and patients using a new generation adaptive optics scanning laser ophthalmoscope. *Biomed Opt Express*. 2011; 2:2189–2201. [PubMed: 21833357]
18. Duncan JL, Zhang Y, Gandhi J, Nakanishi C, Othman M, Branham KE, Swaroop A, Roorda A. High-resolution imaging with adaptive optics in patients with inherited retinal degeneration. *Invest Ophthalmol Vis Sci*. 2007; 48:3283–3291. [PubMed: 17591900]
19. Wolfing JI, Chung M, Carroll J, Roorda A, Williams DR. High-resolution retinal imaging of cone-rod dystrophy. *Ophthalmology*. 2006; 113:1014–1019.
20. Choi SS, Doble N, Hardy JL, Jones SM, Keltner JL, Olivier SS, Werner JS. In vivo imaging of the photoreceptor mosaic in retinal dystrophies and correlations with visual function. *Invest Ophthalmol Vis Sci*. 2006; 47:2080–2092. [PubMed: 16639019]
21. Chen Y, Ratnam K, Sundquist SM, Lujan B, Ayyagari R, Gudiseva VH, Roorda A, Duncan JL. Cone photoreceptor abnormalities correlate with vision loss in patients with stargardt disease. *Invest Ophthalmol Vis Sci*. 2011; 52:3281–3292. [PubMed: 21296825]
22. Futoshi H, Koji N, Ken-ichi S, Yasuyuki N. A compact adaptive optics scanning laser ophthalmoscope with high-efficiency wavefront correction using dual liquid crystal on silicon-spatial light modulator. *Proc SPIE*. 2011; 7885:788515.
23. Marmor MF, Fulton AB, Holder GE, Miyake Y, Brigell M, Bach M. International society for clinical electrophysiology of vision. ISCEV standard for full-field clinical electroretinography—2008 update. *Doc Ophthalmol*. 2009; 1:69–77. [PubMed: 19030905]
24. Audo I, Michaelides M, Robson AG, Hawlina M, Vaclavik V, Sandbach JM, Neveu MM, Hogg CR, Hunt DM, Moore AT, Bird AC, Webster AR, Holder GE. Phenotypic variation in enhanced S-cone syndrome. *Invest Ophthalmol Vis Sci*. 2008; 49:2082–2093. [PubMed: 18436841]
25. Escher P, Gouras P, Roduit R, Tiab L, Bolay S, Delarive T, Chen S, Tsai CC, Hayashi M, Zernant J, Merriam JE, Mermod N, Allikmets R, Munier FL, Schorderet DF. Mutations in NR2E3 can cause dominant or recessive retinal degenerations in the same family. *Hum Mutat*. 2009; 30:342–351. [PubMed: 19006237]
26. Wang NK, Fine HF, Chang S, Chou CL, Cella W, Tosi J, Lin CS, Nagasaki T, Tsang SH. Cellular origin of fundus autofluorescence in patients and mice with a defective NR2E3 gene. *Br J Ophthalmol*. 2009; 93:1234–1240. [PubMed: 19429590]
27. Marmor MF, Jacobson SG, Foerster MH, Kellner U, Weleber RG. Diagnostic clinical findings of a new syndrome with night blindness, maculopathy, and enhanced S-cone sensitivity. *Am J Ophthalmol*. 1990; 110:124–134. [PubMed: 2378376]
28. Pachydaki SI, Klaver CC, Barbazetto IA, Roy MS, Gouras P, Allikmets R, Yannuzzi LA. Phenotypic features of patients with NR2E3 mutations. *Arch Ophthalmol*. 2009; 127:71–75. [PubMed: 19139342]
29. Haider NB, Naggert JK, Nishina PM. Excess cone cell proliferation due to lack of a functional NR2E3 causes retinal dysplasia and degeneration in rd7/rd7 mice. *Hum Mol Genet*. 2001; 10:1619–1626. [PubMed: 11487564]
30. Ooto S, Hangai M, Takayama K, Sakamoto A, Tsujikawa A, Oshima S, Inoue T, Yoshimura N. High-resolution imaging of the photoreceptor layer in epiretinal membrane using adaptive optics scanning laser ophthalmology. *Ophthalmology*. 2011; 118:873–881. [PubMed: 21074858]
31. Bessho K, Fujikado T, Mihashi T, Yamaguchi T, Nakazawa N, Tano Y. Photoreceptor images of normal eyes and of eyes with macular dystrophy obtained in vivo with an adaptive optics fundus camera. *Jpn J Ophthalmol*. 2008; 52:380–385. [PubMed: 18991039]
32. Mustafi D, Kevany BM, Genoud C, Okano K, Cideciyan AV, Sumaroka A, Roman AJ, Jacobson SG, Engel A, Adams MD, Palczewski K. Defective photoreceptor phagocytosis in a mouse model of enhanced S-cone syndrome causes progressive retinal degeneration. *FASEB J*. 2011; 25:3157–3176. [PubMed: 21659555]
33. Baraas RC, Carroll J, Gunther KL, Chung M, Williams DR, Foster DH, Neitz M. Adaptive optics retinal imaging reveals Scone dystrophy in tritan color-vision deficiency. *J Opt Soc Am A Opt Image Sci Vis*. 2007; 24:1438–1447. [PubMed: 17429491]

34. Marmor MF, Tan F, Sutter EE, Bearnse MA Jr. Topography of cone electrophysiology in the enhanced S-cone syndrome. *Invest Ophthalmol Vis Sci.* 1999; 40:1866–1873. [PubMed: 10393063]

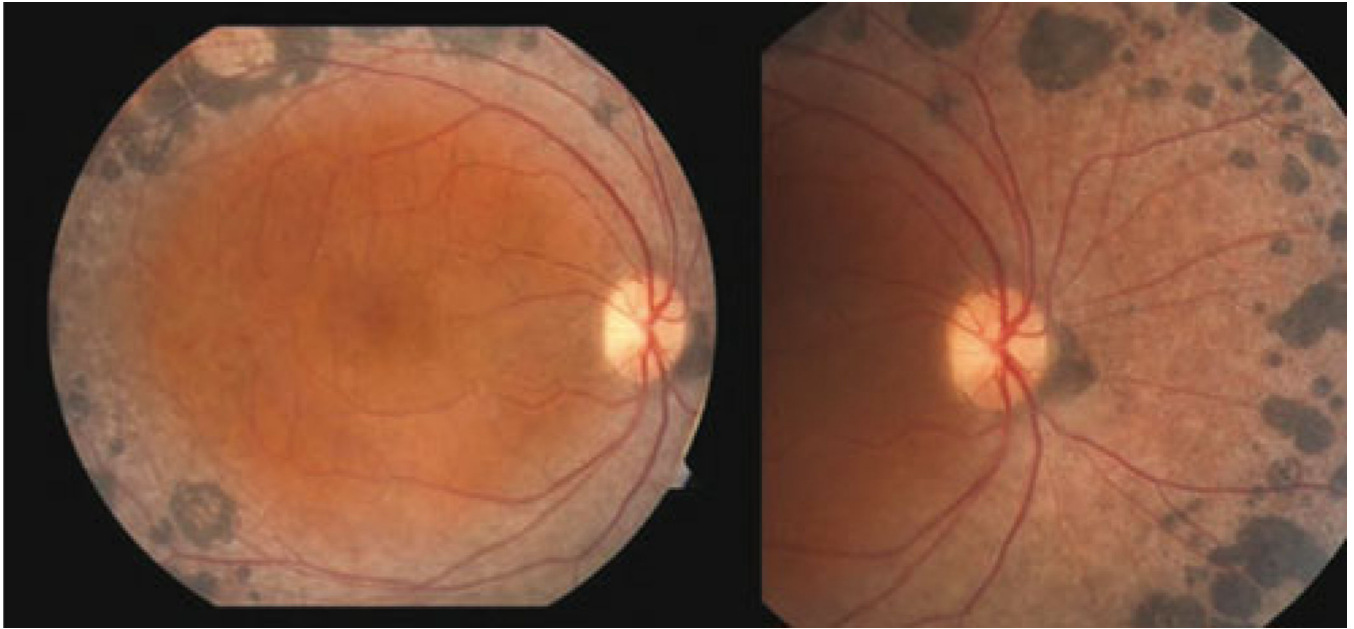


Fig. 1. The fundus photograph of the right eye from patient 1. Extensive subretinal nummular pigmentation, located mostly in the mid-periphery along the vascular arcades, is visible. There is no indication of peripheral or central retinoschisis or maculopathy. No additional abnormal findings were found within the vascular arcades

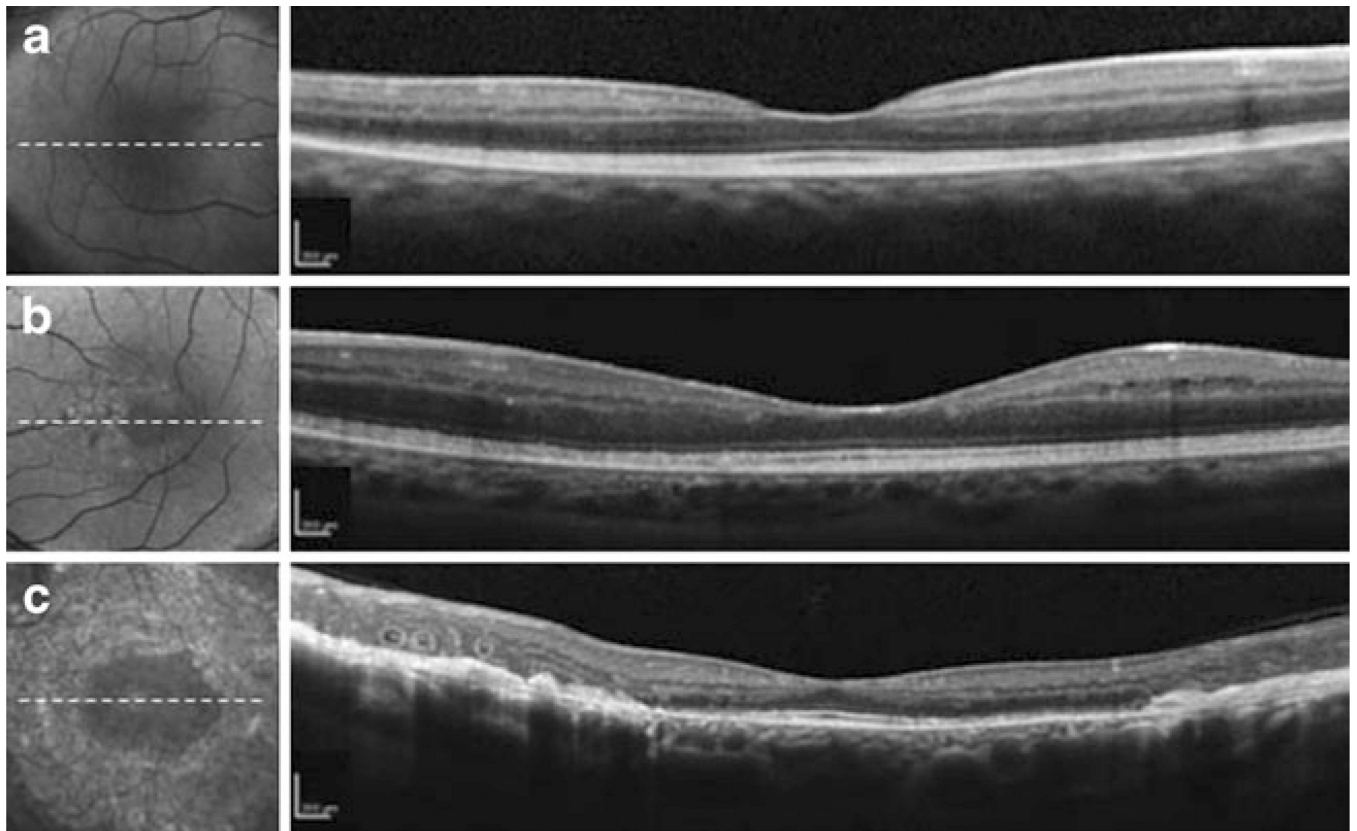


Fig. 2. Macular SD-OCT images. **a** Patient 1 image corresponding to the dotted white line in the FAF image. Note the hypo-autofluorescent clumping coincident with outer peripheral nummular pigmentation along the outer vascular arcades. A decrease in the overall retinal thickness was observed, and there was no cystoid macular edema or foveal schisis. **b** Patient 2 scan corresponding to the dotted white line in the FAF image. FAF image shows hypo-autofluorescent clumping coincident with nummular pigmentation and hyper-autofluorescence within the parafovea, more prominent nasal to the macula. FAF imaging correlated in cross-sectional SD-OCT scans. **c** Patient 3 image corresponding to the dotted white line in the IR image. A slightly disrupted IS/OS line can be seen in the parafoveal area, as well as distinct white spots, retinal fibrosis, and perimacular atrophy within the pigmented area

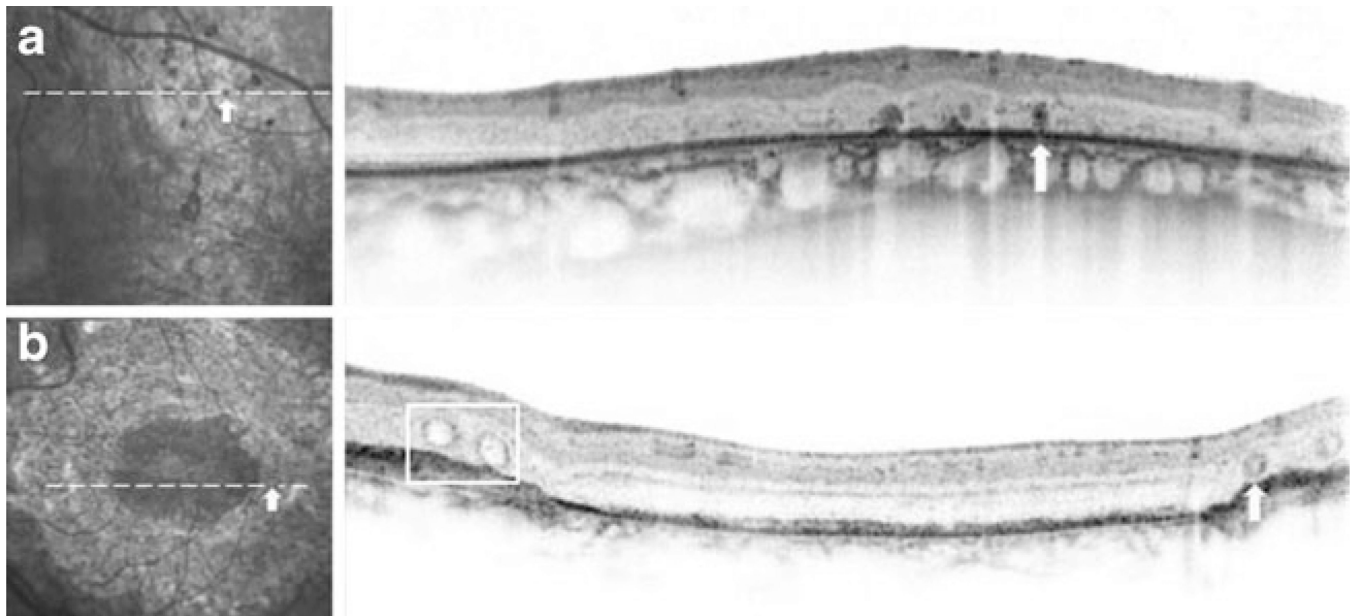
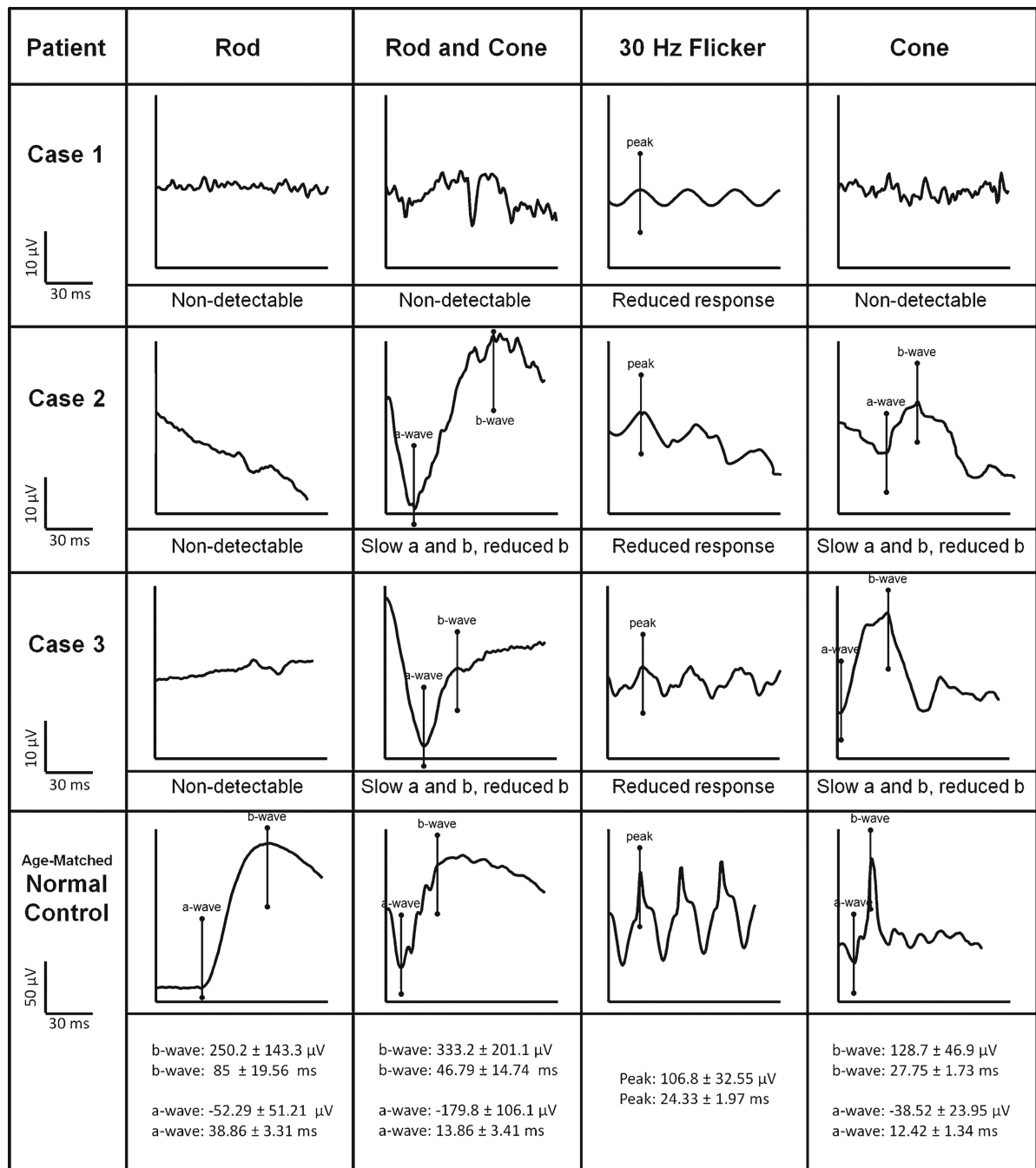


Fig. 3. Peripheral SD-OCT images from patients 2 and 3. **a** Magnified view of nummular pigment deposits in an IR image of patient 2, with the corresponding SD-OCT scan across a single subretinal pigment clump (*white arrow*). A dark, oval-shaped pigmented lesion is shown on IR and SD-OCT images. **b** Rosette-like lesion (*white arrow*) and retinal tubulation (*white box*) identified in the SD-OCT image of the left eye of patient 3. Note the appearance of the rosette-like lesion and the cross sections of observed hollow retinal tubulation

**Fig. 4.**

ISCEV-standard ERG tracings of each enhanced S-cone study patient. Rod-specific, maximal mixed rod and cone, 30-Hz flicker stimulus, and transient single-cone ERG waveforms are shown. The scales, with normal ranges for each condition, are listed in the bottom row. The ERG responses to a standard single flash (*cone*) had similar waveforms under photopic (*cone*) and maximal scotopic conditions, except in waveform amplitude. The 30-Hz flicker stimulus waveforms have reduced amplitudes compared to single flash photopic (*cone*) a-waves

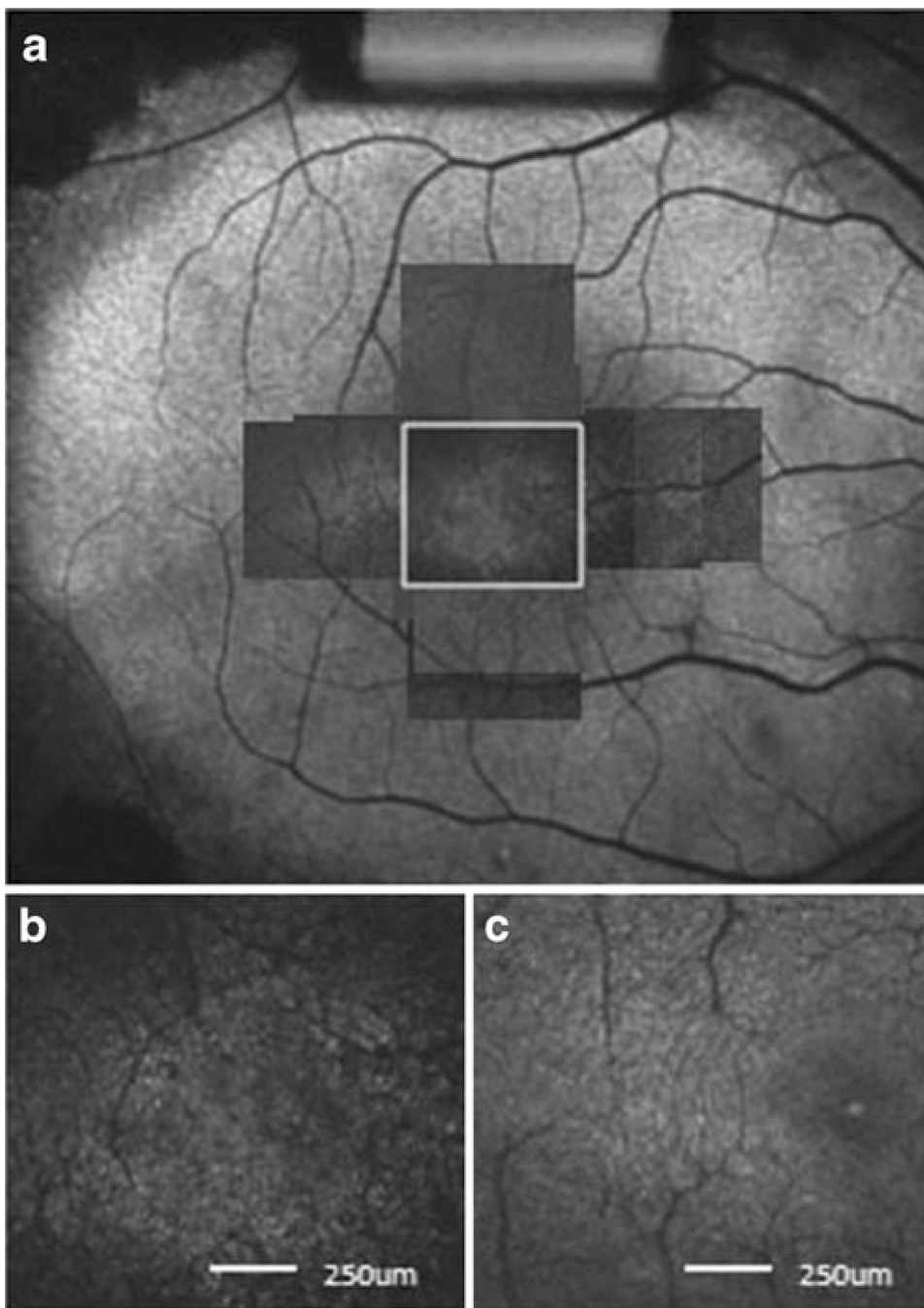


Fig. 5. The AO-SLO image of patient 1. **a** A montage of AO-SLO images from patient 1 is matched with the FAF image. **b** Magnification of the area indicated by the *white box* in part a. Dark patchy lesions in the central retina can be seen. The *scale bar* represents 250 μm . **c** An AO-SLO image from a normal subject at the same location and magnification as shown for patient 1. The image from the normal subject has a regular cone mosaic pattern, and no patchy lesions are visible. *Scale bar* represents 250 μm

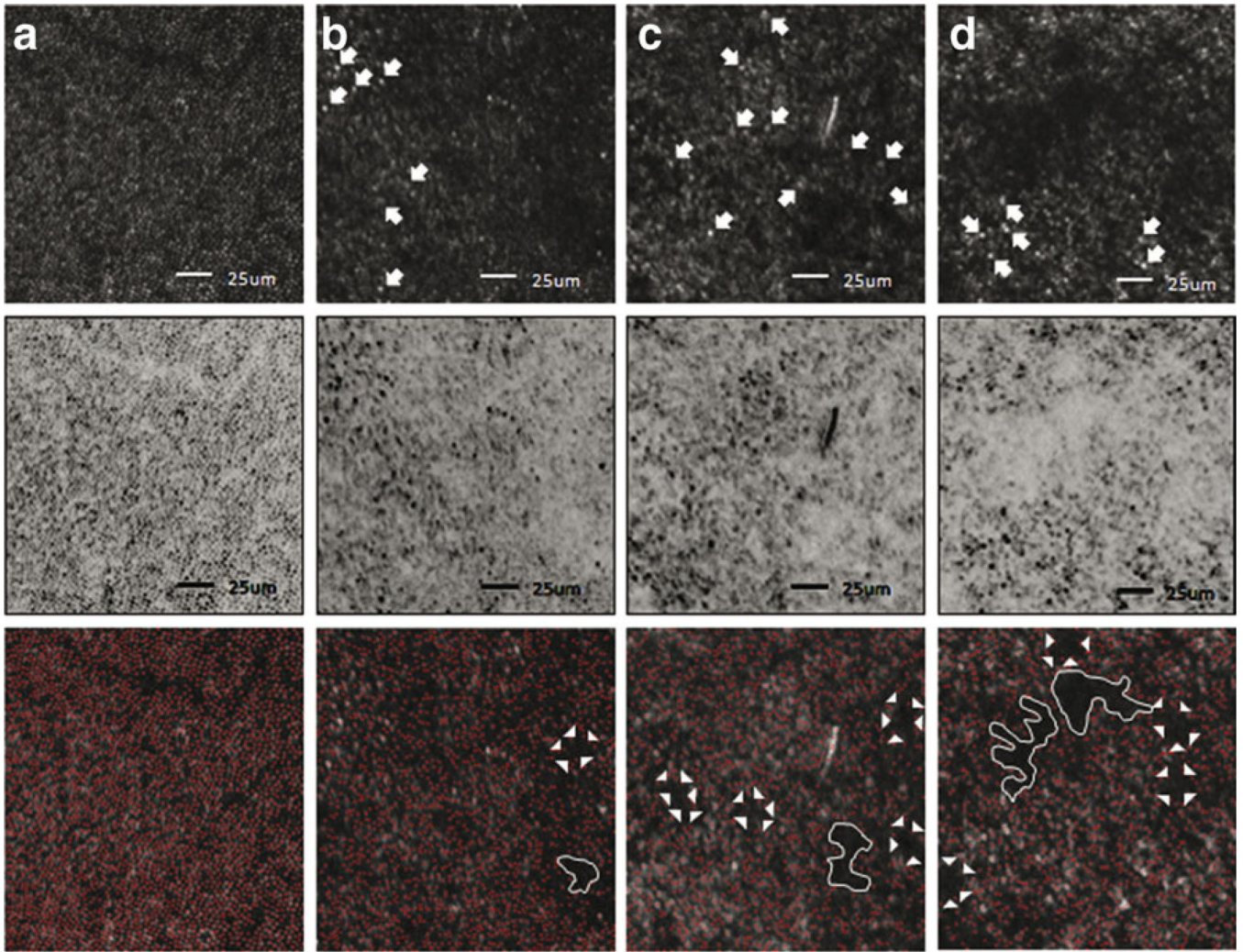


Fig. 6.

Adaptive optics-scanning laser ophthalmoscopy images highlight the appearance of hyporeflective lesions in each study patient. **a** AO-SLO images, from a normal patient 0.5 mm temporal to the foveal center, show a nearly continuous and regular cone mosaic pattern. **b** AO-SLO images of patient 1, 0.5 mm nasal to the foveal center. **c** AO-SLO images of patient 2, 0.5 mm temporal to the foveal center. **d** AO-SLO images of patient 3, 0.5 mm temporal to the foveal center. *Top row* images are the raw AO-SLO images. All patients had interruptions in the continuity of the cone mosaic pattern, along with dark regions, primarily in the center of the retina, where cones were missing or lost. Compared to normal controls, cone cells of ESCS patients were sparsely distributed and were asymmetrical in size and shape. Morphologically disrupted and/or abnormal cone cells are indicated by arrow. Color-inverted images (*center row*) better distinguish the presence and distribution of unaffected cones throughout the imaged mosaic. Software-analyzed images (*bottom row*) to detect cones (*red dots*) to the software enhance the size, shape, and appearance of the sparse distribution and pathognomonic dark lesions. Confluent lesions are

depicted by *white lines* and typical patchy dark lesions are indicated by a *white arrowhead*.
Scale bars represent 250 μm

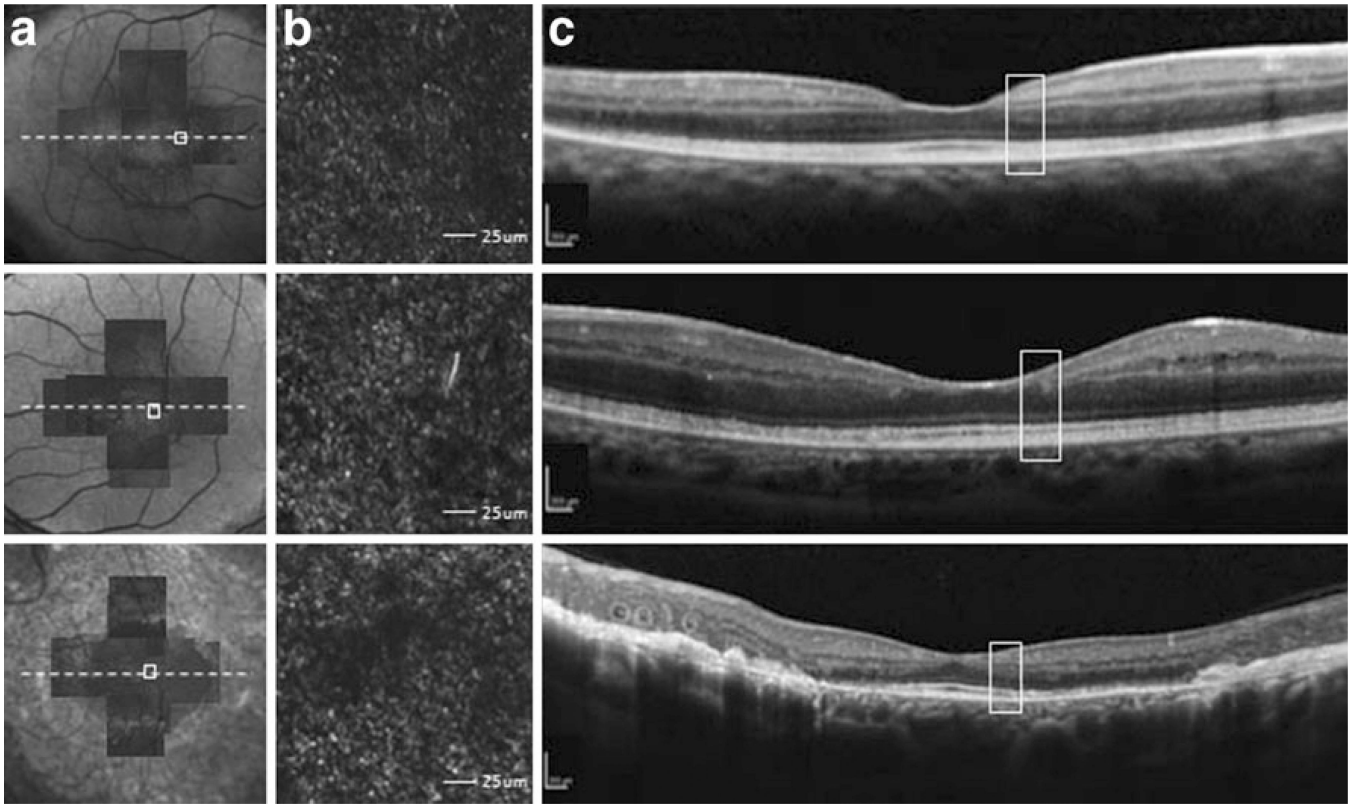


Fig. 7.

Comparison of photoreceptor structure, as represented on AO-SLO and SD-OCT images. **a** Montage of AO-SLO images from each patient is matched with an FAF or IR image. The location of AO-SLO images, and corresponding SD-OCT sections, is marked. **b** All AO-SLO images show sparse distribution and large cell size of cones, along with pathognomonic dark lesions. *Scale bars* represent 25 μm . **c** Areas in SD-OCT images that correspond to AO-SLO images (*white box*) are shown. An intact inner ellipsoid band indicated that the IS/OS junctions were present, and the OS/RPE line was intact. *Scale bars* represent 250 μm

Table 1

Profiles of patients

	Case 1	Case 2	Case 3
Sex	Female	Female	Female
Age (years)	34	33	25
Ethnicity	Hispanic	Caucasian	Caucasian
Imaged eye	OD	OS	OS
BCVA	20/30	20/50	20/20
Subjective refraction	Sph: +6.25	Sph: +0.75	Sph: +2.0
	Cyl:+0.5	Cyl:+0.5	Cyl: -2.0
Axial length (mm)	19.78	22.53	21.43
ACD depth (mm)	3.06	3.75	3.31
NR2E3 mutation	363C>T	119-2A>C	932G>A
	IVS1-2A>C	202A>G	932G>A

BCVA best-corrected visual acuity, *ACD* anterior chamber depth